THE LCLS-II-HE, A HIGH ENERGY UPGRADE OF THE LCLS-II*

T.O. Raubenheimer[†], for LCLS-II/LCLS-II-HE Collaborations
SLAC National Accelerator Laboratory, Menlo Park, USA

Abstract

The LCLS-II is a CW X-ray FEL covering a photon spectral range from 200 to 5,000 eV. It is based on a 4 GeV SRF linac installed in the 1st km of the SLAC linac tunnel. This paper will describe a high energy upgrade, referred to as the LCLS-II-HE, which will increase the beam energy to 8 GeV and the photon spectral range to 12.8 keV; this range may be extended through 20 keV with improvements of the electron injector and beam transport. The LCLS-II-HE received the US DOE CD-0 approval, Mission Need, and has developed a CDR in support of a CD-1 review scheduled for summer 2018.

INTRODUCTION

The development of X-ray free-electron lasers (XFELs) has launched a new era in X-ray science by providing ultrafast coherent X-ray pulses with a peak brightness that is nearly one billion times higher than previous X-ray sources. As the world's first hard X-ray FEL, the LCLS has already demonstrated tremendous scientific impact across broad areas of science, based on fundamental studies of the behavior of matter at the atomic length scale and femtosecond timescale. A comprehensive scientific overview of the first five years of LCLS operation was recently published [1]. Numerous similar facilities are just beginning operation or are under construction around the world [2].

While the LCLS has delivered unprecedented peak brightness, with a repetition rate of 120 Hz, the average brightness is modest, similar to that of a synchrotron source. Furthermore, many experiments require attenuation of the peak intensity in order to avoid perturbation of the sample by the X-ray probe. In these cases, signal accumulation times often become prohibitive, thus rendering many experiments impractical. The LCLS-II will provide ultrafast X-rays in the soft and tender X-ray range (0.2-5 keV) at repetition rates up to 1 MHz with two independent XFELs based on adjustable-gap undulators: a soft X-ray undulator (SXU) covering the range from 0.2 to 1.3 keV, and a hard X-ray undulator (HXU) covering the range from 1 to 5 keV. This development is driven by important new science opportunities that have been identified and advanced over the past decade through scientific workshops, both in the U.S. and around the world [3].

The extension of the LCLS-II to the hard X-ray regime is motivated by the scientific need for precision measurements of structural dynamics on atomic spatial scales and fundamental timescales. Such measurements are essential for addressing many of the transformative op-

portunities identified in the latest report from the Basic Energy Sciences Advisory Committee (BESAC) [4], and will provide detailed insight into the behavior of complex matter, real-world heterogeneous samples, functioning assemblies, and biological systems on fundamental scales of energy, time, and length. The LCLS-II High Energy Upgrade (LCLS-II-HE) is a natural extension to LCLS-II, extending the high-repetition-rate capabilities into the critically important "hard X-ray" regime (spanning from 5 keV to at least 12.8 keV and potentially up to 20 keV) that has been used in more than 75% of the LCLS experiments to date.

The LCLS-II-HE upgrade will build on the LCLS-II, described in Refs. [5] and [6], and will add significant capability to the facility. The changes in the LCLS-II capability are summarized below and illustrated in Fig. 1.

- The photon spectral range from the hard X-ray undulator at MHz-rate will be extended from 1 – 5 keV to 1 – 12.8 keV using electrons beams with energies between 3.3 and 8 GeV with the possibility of X-ray energies approaching 20 keV given the success of off-project R&D programs;
- The hard X-ray undulator will include the capability for self-seeding the MHz-rate X-ray beam;
- The soft X-ray undulator will be able to produce X-rays between 0.2 and 1.3 keV or access the tender X-ray region between 1 – 5 keV at MHz-rates coincidently with the production of MHz-rate hard X-rays;
- The hard X-ray beamlines and instruments will be upgraded to maximize the science from the MHz-rate high energy FEL beams;
- And, the hard X-ray experimental hall will be modified to incorporate an additional experimental instrument and also better optimize the usage of the existing instruments;
- The performance of LCLS and LCLS-II operational modes and techniques will not be negatively impacted by the LCLS-II-HE including the generation of X-ray pulses with high peak power (100's of GW) at 120 Hz using the copper linac.

The layout of the LCLS-II-HE accelerator is shown schematically in Fig. 2. The facility will use the existing accelerator tunnels at SLAC. The increase in beam energy from LCLS-II to LCLS-II-HE is due to an increase in acceleration gradient and an increase in the SRF linac length. In particular, the SRF linac will be extended to fill the first km of the existing SLAC linac tunnel which has been largely cleared of legacy equipment.

To construct the LCLS-II-HE, SLAC will continue the partnership with other national laboratories having recent technical leadership in the critical SRF technologies. In a

process similar to that pursued by the LCLS-II project, the partner laboratories will be responsible for delivering significant portions of the project scope to SLAC. Cornell University, FNAL, and JLab will be engaged with increasing the accelerating gradient of the accelerator

cavities for new cryomodules while the SRF linac and associated systems are expected to be provided by a combination of FNAL and JLab which have the experience of producing the LCLS-II cryomodules.
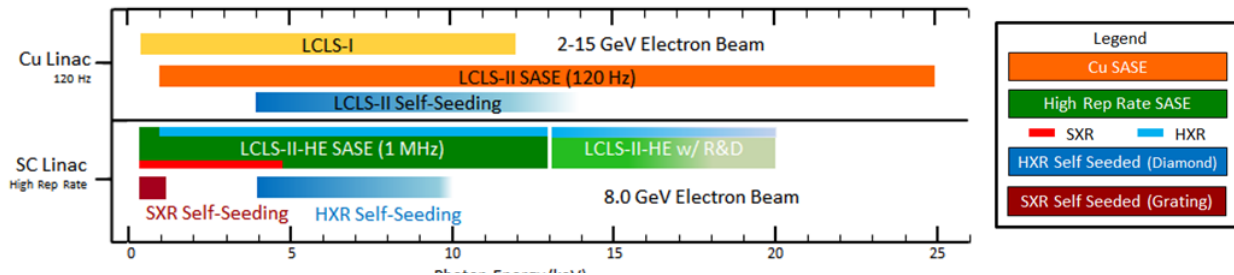
Figure 1: Photon energies from the SRF and CuRF linacs for both SASE and self-seeded operation, assuming 8.0 GeV SRF electrons and 3-to-15 GeV CuRF electron beams. Access to higher photon energies from the CuRF or SRF linacs will be possible given the success of off-project R&D programs.
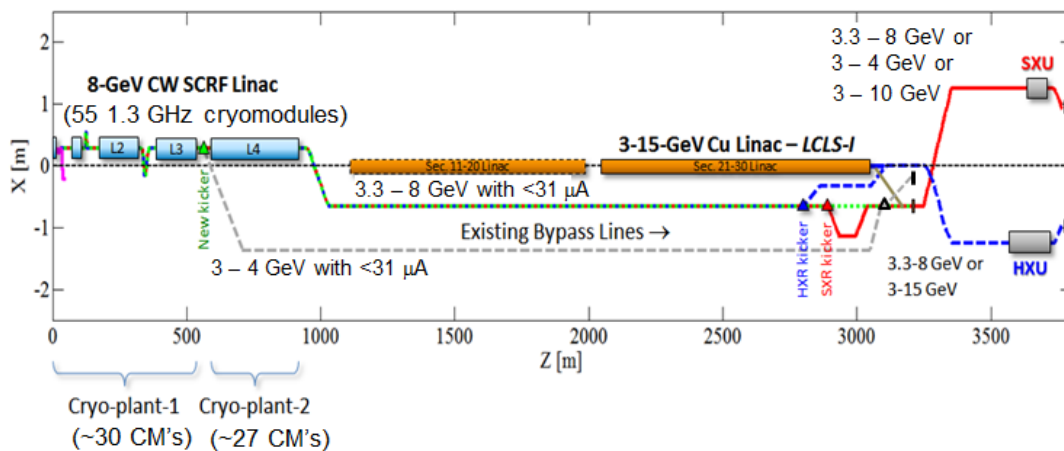
Figure 2: Layout of the LCLS-II-HE facility with 8 GeV at the end of the SRF-Linac and 15-GeV in the normal-conducting linac. An additional 3.8-GeV pulsed extraction line is included to allow a low-energy extraction into the SXU FEL while the HXU FEL runs with high energy (3.3-8 GeV or 3-15 GeV) electrons.

ACCELERATOR PARAMETERS

The primary challenge for the LCLS-II-HE is achieving the high rate performance at 12.8 keV. The LCLS-II is designed to deliver 5 keV photons with a beam energy of 4 GeV and thus, based on the FEL photon energy scaling with γ^2, one would expect that 13 keV could be attained with a beam energy of 6.5 GeV. However, at these short wavelengths, the FEL performance is limited by the beam emittance in the undulator. Given the expected performance of the LCLS-II injector and the LCLS-II HXR undulator, a minimum beam energy of 8 GeV is required to generate 13 keV FEL photons.

The design of the LCLS-II left an opportunity to upgrade the linac energy by installing additional cryomodules and also by increasing the acceleration gradient. The LCLS-II cavities and cryomodules are being qualified at 19 MV/m but the LCLS-II operating specification is

~15.5 MV/m. The SLAC tunnel has 250 meters of empty space following the SRF linac in which 20 additional cryomodules can be added. With cavities operating at an average $Q_0 \approx 2.7 \times 10^{10}$, the cryoplant will allow operation of the extended linac at an average gradient of ~19.4 MV/m to achieve an 8-GeV electron beam, doubling the energy at the linac end and extending the spectral range of the MHz-rate FEL to 13 keV.

To achieve the desire Q_0, an implementation of the nitrogen-doping [7] process was developed for the LCLS-II. The process adopted by LCLS-II [8,9,10] is producing cavities with average performance better than specified. On average, cavities in vertical test can achieve an average maximum gradient >20 MV/m with an average $Q_0 > 3 \times 10^{10}$ as illustrated in Fig. 3. After installation in the cryomodules, the maximum gradient appears to
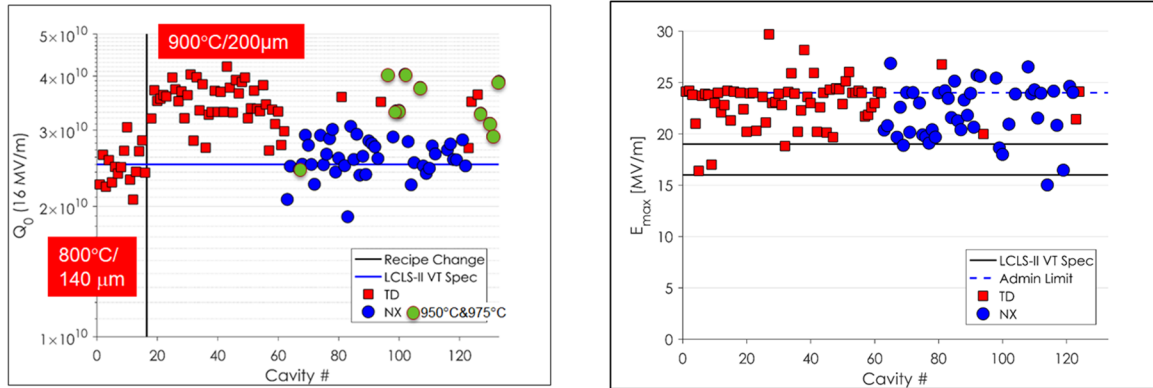
Figure 3: Left: LCLS-II cavity Q0 measured at the nominal 16 MV/m gradient; the vertical line indicates a change in bake temperature and a few cavities have been treated at >950 °C as indicated in the plot legend. Right: Maximum LCLS-II cavity gradient achieved in the vertical testing. Note that a 24 MV/m administrative gradient limit was imposed in many cases.

decrease by 10~15% which is consistent with results observed at the European XFEL (EuXFEL) [11]. It is expected that the LCLS-II cryomodules should be robust at an average gradient of 18 MV/m.

Figure 4: Expected SRF gradient performance as a function of N_2 doping temperature and time based on a simulation from Ref [12].

The LCLS-II N_2-doping choice was chosen to maximize the Q_0 at 16 MV/m. As illustrated in Fig. 4, it is expected that a small variation in the doping procedure would yield still higher gradients at the expense of Q_0. An R&D program will be initiated to establish a gradient of 24.5 MV/m at $Q_0 > 2.7 \times 10^{10}$.

The LCLS-II-HE cryomodule will be the same as those for the LCLS-II which were designed at Fermilab and are based heavily on the EuXFEL design. The assembly and installation procedures will be adopted from those developed for the EuXFEL.

The main operating parameters for the LCLS-II-HE SRF linac are listed in Table 1, along with those of the LCLS-II SRF linac. The number of 1.3-GHz cryomodules is increased from 35 to 55 and the gradient of most of the LCLS-II cryomodules is increased from ~16 to 18 MV/m

while the gradient in the 20 new LCLS-II-HE cryomodules would be further increased to 20.8 MV/m. The maximum average beam power delivered by the linac would be increased to 375 kW, which could consist of 31 μA at 8 GeV and 31 μA at 3.8 GeV in the 2nd bypass line discussed below.

ACCELERATOR LAYOUT

In operation, the LCLS-II-HE upgrade will want to simultaneously support a soft X-ray program with photons between 0.2 and 1.3 keV and a hard X-ray program with X-rays between 1 and 13 keV. Assuming the LCLS-II-HE upgrade reuses the LCLS-II SXR and HXR undulators, this could be facilitated by extracting some of the beam at an energy between 3 and 4 GeV for the soft X-ray program while accelerating the rest to a final energy between 3.3 and 8 GeV for the hard X-ray program. Thus, a mid-point extraction of a 'low energy' beam will be included.

A schematic of LCLS-II-HE is illustrated in Fig. 2, where an additional pulsed extraction line is added after linac segment L3 to transport ~3.8-GeV beam to the SXR undulator (dashed gray line) and a new linac segment, L4, follows to accelerate the undeflected beam to 8 GeV. The energy upgrade will add 20 new cryomodules, each having essentially the same design as those being developed for the LCLS-II, to generate the 8-GeV electron beam. This upgrade reuses the LCLS-II injector, linac, cryoplants, undulators, beam transport systems, and existing tunnels. The implementation will require some modification to the cryogenic distribution system which is shown in Fig. 5, the addition of a new extraction point for the ~3.8-GeV beam, which will be injected into an existing bypass line (gray-dashed line in Fig. 2), and a new beam dump at the end of this transport line.

The new ~3.8 GeV extraction enables the LCLS-II-HE to operate with essentially three independent sources of electrons: those from the end of L3 at ~3.8 GeV, those from the end of L4 where the electron energy can range

from 3.3 to 8 GeV, and those from the 120 Hz copper linac (CuRF) with a beam energy between 3 and 15 GeV.

The design is based on the LCLS-II injector [13] and the bunch compression system. No hardware changes will be made upstream of the middle of the LCLS-II L3 and the configuration of the injector, L0, laser heater, L1, and BC1 will be identical to that designed for LCLS-II. There are three reasons for this: (1) extensive optimization of the LCLS-II injector and bunch compression sys-tem has been performed [14,15] and the LCLS-II-HE upgrade will reuse much of this effort; (2) radiation shielding for backward traveling dark current is challeng-ing around the LCLS-II gun and laser and it will likely need to be increased with changes to the gradient in L0 and L1; and (3) the beam energy is low in this region so energy stability and reliability is important, which a lower gradient tends to afford.

Table 1: LCLS-II and LCLS-II-HE SRF Linac Parameters

SCRF-Linac Parameters	LCLS-II	LCLS-II-HE	Unit
Final electron energy	3.3 - 4.0	3.3 - 8.0	GeV
Electron energy at L3/L4 extraction point	-	3.3 - 4.0	GeV
Electron Bunch Charge	$0.01 - 0.30$	$0.01 - 0.30$	nC
Max. bunch repetition rate	929	929	kHz
Average electron beam power in L2-L4	<0.25	<0.25	MW
Average electron power in BSY	<0.25	<0.375	MW
Max. avg. electron current in L0-L3	62	62	μA
Max. avg. electron current in L4	--	31	μA
Max. avg. electron current in Low Energy Extraction line	--	31	μA
Total Number of 1.3-GHz Cryomodules	35	55	-
Total Number of 3.9-GHz Cryomodules	2	2	-
Installed 1.3 GHz RF Voltage	4.65	8.64	GeV
Active SCRF accelerator length	296	462	m
1.3 GHz Cryomodules in L0, L1, L2, L3	1, 2, 12, 20	1, 2, 12, 13	-
1.3 GHz Cryomodules in L4	--	27	-
RF Overhead (spare cavities)	6.1	4.1	%
Mean RF Gradient in powered cavities: L0-L1	< 16.0	< 16.0	MV/m
Mean RF Gradient in powered cavities: L2-L3	< 16.0	18.0	MV/m
Mean RF Gradient in powered LCLS-II cavities: L4	--	18.0	MV/m
Mean RF Gradient in powered LCLS-II-HE cavities: L4	--	20.8	MV/m
Installed 2K cryo-capability	8.0	8.0	kW
Expected heat load at max energy: L0-L3	3.7	3.5	kW
Expected heat load at max energy: L4	-	3.8	kW
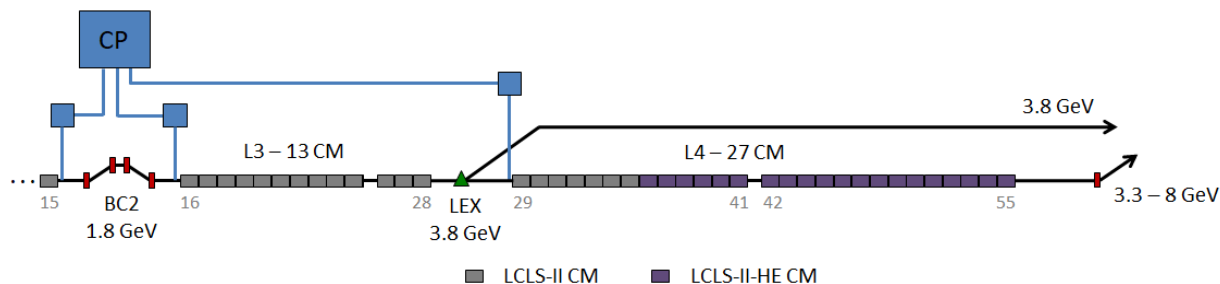
Figure 5: LCLS-II-HE SRF expansion and layout. Each gray block represents one 12-m long 1.3-GHz cryomodule (CM), with 55 total CM's. A fast extraction kicker is added at 3.8-GeV to optionally feed the SXU FEL at 3.8 GeV. The cryo-distribution (CP – blue lines) is also shown. CM's upstream of BC2 are not shown.

EXPERIMENTAL SYSTEMS

The LCLS-II-HE upgrade will also require a revision to the existing X-ray instrument suite. This involves three different types of upgrades/modifications: (i) repetition rate enhancements (X-ray optics, detectors, lasers, data systems) consistent with the high average power beam and pulse rate, (ii) relocations to maximize experiment capacity and operational efficiency, and (iii) new instru-mentation to augment present capabilities.

The configuration of the Far Experimental Hall for LCLS-II-HE is illustrated in Fig. 6. The revised instrument plan includes:

• Modifying the Far Experimental Hall (FEH) to accommodate an additional X-ray hutch

• Replacing the XCS instrument with a new instrument (Dynamic X-ray Scattering, DXS) designed for both high-resolution inelastic X-ray scattering and X-ray photon correlation spectroscopy

• Bifurcating the present CXI instrument into two beamline branches and hutches (with two micro-focus chambers and a nano-focus chamber) to improve efficiency and optimize high-sensitivity experimental techniques

• Relocating the MFX instrument on a new branch line to improve efficiency

• Relocating the MEC instrument to a new, shielded location to permit higher-power laser-matter interactions

• Adapting the design of the Tender X-ray Imaging (TXI) instrument in hutch NEH1.2 for LCLS-II, extending its energy reach to combine tender and hard X-ray beams.
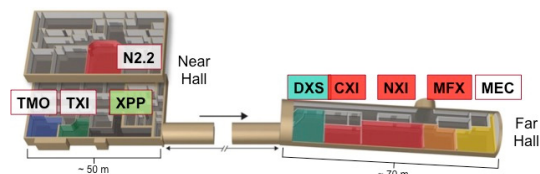
Figure 6: Schematic layout of the LCLS X-ray experimental end stations at the completion of the LCLS-II-HE project, with the Far Experimental Hall reconfigured to include one additonal hutch.

PERFORMANCE SIMULATIONS

Start-2-End (S-2-E) simulations have been performed for the LCLS-II using *IMPACT-T* and *IMPACT-Z* [16,17] and *Genesis* [18]. Included in the tracking are 3D space charge forces, longitudinal wakefields in the linac, CSR in the bends and relevant drift sections, incoherent synchrotron radiation (ISR) in the bends, second-order optics (*e.g.*, chromatic and geometric effects), resistive-wall wakefields in the undulators, and 3D time-dependent FEL simulations [19]. To accurately model the shot-noise in the electron beam in these simulations, the number of macro-particles that are used is equal to the actual number of electrons.

At this time, the hard X-ray simulations are performed using the LCLS-II S-2-E beam distributions at 4 GeV from IMPACT [20,21,19] scaled to the 8 GeV beam energy. This approach is believed to be conservative as most of the deleterious effects such as Longitudinal Space Charge (LSC) force and Coherent Synchrotron Radiation (CSR) which drive the microbunching instability will be moderated by the higher beam energy in the Bypass line.

The FEL performance simulations start from these scaled LCLS-II beams for 100 pC or 20 pC and use *Genesis* to calculate the expected FEL gain and radiation properties. In all these simulations, the post-saturation taper is optimized in *Genesis* using time-dependent simulations which makes the evaluations computationally intensive. An example from the upper end of the tuning range at 12.8 keV with a 20 pC beam are shown in Fig. 7.

The expected average brightness from the LCLS-II-HE is illustrated in Fig. 8 where the purple curves illustrated the expected LCLS-II performance and the red solid curve shows the expected LCLS-II-HE performance at 8 GeV. These calculations are based on the expected performance of the unmodified LCLS-II injector. The dashed red curve shows the performance increased that would arise from a factor of four improvement in the beam emittance at the undulator which might be possible as a result of an injector R&D program.
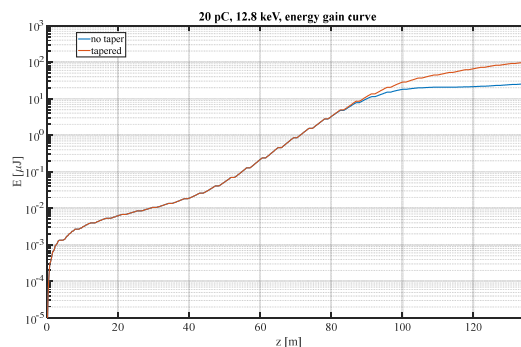
Figure 7: Genesis simulation of X-ray pulse energy at 12.8 keV from a 20 pC LCLS-II bunch scaled to 8 GeV at the HXR undulator.
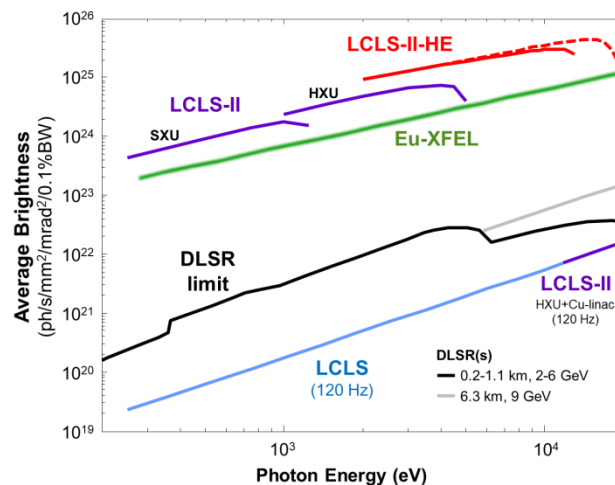
Figure 8: Expected average brightness from LCLS-II and LCLS-II-HE.

ACKNOWLEDGEMENTS

REFERENCES

[1] C. Bostedt, S. Boutet, D. M. Fritz, et al., Reviews of Modern Physics 88, 015007 (2016).

[2] I. Schlichting, W. E. White, and M. Yabashi, J. Synchrotron Radiat. 22, 471 (2016).

[3] "New Science Opportunities enabled by LCLS-II X-ray Lasers," (https://portal.slac.stanford.edu/sites/lcls_public/ Documents/LCLS-IIScienceOpportunities_final.pdf, 2015).

[4] J. C. Hemminger, "Challenges at the Frontiers of Matter and Energy: Transformative Opportunities for Discovery Science - BESAC Report U.S. D.O.E.," (http://science.energy.gov/~/media/bes/besac/pdf/Reports/ CFME_rpt_print.pdf, 2015).

[5] J. N. Galayda, Proc. of IPAC'14, Dresden, Germany, p. 935 (2014).

[6] LCLS-II Technical Design Report, T.O. Raubenheimer, ed. (2017).

[7] A. Grassellino, et al., "Nitrogen and argon doping of niobium for superconducting radio frequency cavities: A pathway to highly efficient accelerating structures," Supercond. Sci. Technol. 26, 102001 (2013).

[8] A. Crawford, et al, "The joint high Q0 program for LCLS-II," Proc. of IPAC 14, Dresden, Germany, p. 2627 (2014).

[9] D. Gonnella, et al, "Nitrogen-doped 9-cell cavity performance in a test cryomodule for LCLS-II," J. Appl. Phys. 117, 023908 (2015).

[10] D. Gonella, et al, Nucl. Instr. And Meth. A, 883, 143-150 (2018).

[11] N. Walker, et al., "Performance analysis of the European XFEL SRF cavities, from vertical test to operation in the modules," WE1A04, Proc. Linac 2016, East Lansing, MI (2016).

[12] D. Gonnella. The Fundamental Science of Nitrogen-Doping of Niobium Superconducting Cavities. PhD Thesis. Cornell University (2016).

[13] F. Zhou, et al., "the LCLS-II njector beamline design and RF coupler correction," MOP021, Proc. of FEL'15, Daejeon, Korea (2015).

[14] G. Marcus and J. Qiang, LCLSII-TN-17-04 (2017).

[15] G. Marcus et al., TUP007, FEL'2015, Daejon, Korea (2015).

[16] J. Qiang et al., *J. Comput. Phys.*, **163**, 434 (2000).

[17] J. Qiang et al., *Phys. Rev. ST Accel. Beams*, **9**, 044204 (2006); J. Qiang et al., *Phys. Rev. ST Accel. Beams*, **12**, 100702 (2009).

[18] S. Reiche, et. al., Start-To-End Simulation for the LCLS X-ray FEL, *Nuclear Instruments and Methods in Physics Research*, **A483** 70 (2002).

[19] G. Marcus and J. Qiang, LCLSII-TN-17-04 (2017).

[20] G. Marcus et al., TUP007, FEL'2015, Daejon, Korea (2015).

[21] J. Qiang et al., WEP070, FEL'2015, Daejon, Korea (2015); J. Qiang, WEA3IO02, NAPAC'2016, Chicago, USA (2016).